

Wind-induced responses of supertall buildings considering soil-structure interaction

Yajun Huang^a and Ming Gu*

State Key Laboratory of Disaster Reduction in Civil Engineering,
Tongji University, 1239 Siping Road, Shanghai, China

(Received December 12, 2017, Revised March 13, 2018, Accepted April 4, 2018)

Abstract. In this study, a simplified three-dimensional calculation model is developed for the dynamic analysis of soil-pile group-supertall building systems excited by wind loads using the substructure method. Wind loads acting on a 300-m building in different wind directions and terrain conditions are obtained from synchronous pressure measurements conducted in a wind tunnel. The effects of soil-structure interaction (SSI) on the first natural frequency, wind-induced static displacement, root mean square (RMS) of displacement, and RMS of acceleration at the top of supertall buildings are analyzed. The findings demonstrate that with decreasing soil shear wave velocity, the first natural frequency decreases and the static displacement, RMS of displacement and RMS of acceleration increase. In addition, as soil material damping decreases, the RMS of displacement and the RMS of acceleration increase.

Keywords: soil-structure interaction; dynamic responses; wind load; supertall building; pile group

1. Introduction

In the present day we are experiencing an unprecedented level of activity in the design and construction of supertall buildings, such as Taipei 101 and Burj Khalifa (Irwin 2009). Wind resistance is one of the most important issues at the design stage for supertall buildings because of their high structural flexibility and the remarkably increased wind speed at higher altitudes. In conventional engineering practice, buildings are often assumed to be fixed at the base, which can be considered reasonable for low-rise buildings on relatively stiff soils. However, for supertall buildings resting on soft soils, they are high-slenderness and low-stiffness dynamic systems involving complex interaction between the wind and soil, similar to wind turbine towers. When soil and foundation flexibility are taken into account, the natural frequencies and total damping are modified (Shirzadeh *et al.* 2013, Rong *et al.* 2017), and the structure's wind-induced responses are affected (Adhikari and Bhattacharya 2011). Thus soil-structure interaction (SSI) effects should be considered while analyzing wind-induced responses of supertall buildings.

There are two approaches to account for SSI in the dynamic analysis of structures, namely, the substructure method (Wolf 1985) and the direct method. In the substructure method, the global system is subdivided into two subsystems: the superstructure and the substructure. Each subsystem is modeled independently and the general structure is formed by connecting these individual

subsystems through the adjacent interface. Some researchers have adopted the substructure method to analyze the effect of SSI on the wind-induced response of tall structures. For example, Novak (1974b), Howell (1978), Galsworthy and El Naggar (2000) examined the effect of SSI on the response of tall reinforced concrete chimneys to gusting wind and vortex shedding; Gorski and Chmielewski (2008) compared along and across-wind responses of a tall chimney with and without flexibility of soil; Lin and Wu (1984), Novak and Hifnawy (1988) included flexible soil in their analysis of tall buildings' vibrations under wind loads; Halabian *et al.* (2003) further adopted a probabilistic approach to evaluate the effects of uncertainties of the value of soil shear wave velocity on the response of RC tall structures; Venanzi *et al.* (2014) introduced an inelastic, 6-degree-of-freedom (DOF) macro-element that accounts for the non-linear and irreversible behavior of the soil-foundation system; and Xu and Kwok (1992) and Liu *et al.* (2008) presented frequency-domain and time-domain analyses separately to calculate the wind-induced vibration of high-rise buildings with tuned mass dampers (TMDs) with consideration of SSI. In the direct approach, the stiffness of the global system (which includes the structure, foundation and supporting medium) is assembled, and the response is obtained in a single step. Based on this method, the finite element analysis can be easily implemented to consider SSI. Viladkar *et al.* (2006), Jisha *et al.* (2013) and Jayalekshmi *et al.* (2015) proposed the three-dimensional finite element model of the cooling tower/chimney-foundation-soil systems to study the SSI response under the influence of wind loads.

Although studies have been performed on the SSI analysis of tall structures under wind loads, many of them considered chimneys/cooling towers, and few considered supertall buildings. In addition, limited research has been performed in the area of SSI analysis of supertall buildings

*Corresponding author, Professor
E-mail: minggu@tongji.edu.cn

^a Ph.D. Student
E-mail: 102894huang@tongji.edu.cn

with pile group foundations. And wind loads in most research are computed according to the wind load spectrum or codes. Although this approach can be considered reasonable for the along-wind load, it may be not accurate for the across-wind load due to the complexity of the load. Furthermore, the assumption of only considering soil geometric damping and neglecting soil material damping in most research about SSI is not suitable for analyzing wind-induced responses, because wind-induced vibration is a low-frequency vibration and the soil geometric damping is very small or maybe vanish under low-frequency vibration. On the other hand, soil material damping becomes the main damping in soil and affects wind-induced responses a lot.

Therefore, a simplified three-dimensional calculation model was developed for the dynamic analysis of soil-pile group-supertall building systems excited by wind using the substructure method in this paper. The dynamic impedance of pile groups is calculated by combining the dynamic impedance of a single pile obtained using the plane strain method and the dynamic interaction factors. At low frequencies, soil geometrical damping is neglected when calculating the soil reaction to pile vibration. Wind loads in different wind directions and terrain conditions are obtained from synchronous pressure measurements conducted in wind tunnel experiments. The wind-induced responses of supertall buildings obtained from proposed calculation models are compared with those from three-dimensional finite element models to verify the proposed calculation model. Lastly, an analysis is performed on the effect of SSI on the first natural frequency, wind-induced static displacement, RMS of displacement, and RMS of acceleration at the top of supertall buildings.

2. Proposed calculation models

2.1 Soil-foundation-superstructure system

Consider a supertall building supported by pile groups. The superstructure is discretized in n_e beam elements and n_e+1 nodes, and the masses are assumed to be lumped. To model SSI, a single-node (linear elastic) soil-foundation element as the substructure is added at the base of the superstructure, as depicted in Fig. 1.

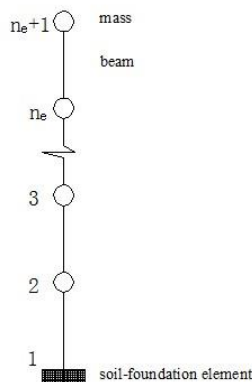


Fig. 1 Soil-foundation-structure-interaction model

Because the visco-elastic model is adopted for the soil, the equations of motion of the soil-foundation-superstructure interaction model cast in the frequency domain are as follows

$$(-\omega^2[M] + i\omega[C] + [K])\{X(\omega)\} = \{F(\omega)\} \quad (1)$$

where $i = \sqrt{-1}$, ω is the circular frequency of oscillation, $[M]$ is the $[n \times n]$ diagonal global mass matrix, $[C]$ is the $[n \times n]$ global damping matrix, $[K]$ is the $[n \times n]$ global stiffness matrix, $\{X(\omega)\}$ is the $[n \times 1]$ vector of the frequency Fourier transform of the nodal displacements, $\{F(\omega)\}$ is the $[n \times 1]$ vector of the frequency Fourier transform of the nodal forces, and n is the number of DOFs. Since every node possesses six degrees of freedom, $n = 6 \times (n_e + 1)$.

Eq. (1) can be written in extended form as follows

$$\begin{pmatrix} -\omega^2 \begin{bmatrix} M_{bb} & 0 \\ 0 & M_{ii} \end{bmatrix} \\ +i\omega \begin{bmatrix} C_{bb} & C_{bi} \\ C_{ib} & C_{ii} + C_{ff} \end{bmatrix} \\ + \begin{bmatrix} K_{bb} & K_{bi} \\ K_{ib} & K_{ii} + K_{ff} \end{bmatrix} \end{pmatrix} \begin{Bmatrix} X_b(\omega) \\ X_i(\omega) \end{Bmatrix} = \begin{Bmatrix} F_b(\omega) \\ 0 \end{Bmatrix} \quad (2)$$

where the common nodes at the superstructure-substructure interface are defined with the i subscript; subscript b defines the other nodes within the superstructure. The subscript ff represents the corresponding parameters for the substructure system (e.g., soil-foundation system). The stiffness and damping of the soil-foundation element (K_{ff} and C_{ff} , respectively) are the frequency-dependent stiffness and damping coefficients in the impedance function of the pile group, which will be introduced in Section 2.2 in detail.

For a supertall building with a fixed base, Eq. (1) can be rewritten as

$$\begin{pmatrix} -\omega^2 \begin{bmatrix} M_{bb} & 0 \\ 0 & M_{ii} \end{bmatrix} \\ +i\omega \begin{bmatrix} C_{bb} & C_{bi} \\ C_{ib} & C_{ii} \end{bmatrix} \\ + \begin{bmatrix} K_{bb} & K_{bi} \\ K_{ib} & K_{ii} \end{bmatrix} \end{pmatrix} \begin{Bmatrix} X_b(\omega) \\ 0 \end{Bmatrix} = \begin{Bmatrix} F_b(\omega) \\ F_i(\omega) \end{Bmatrix} \quad (3)$$

In conjunction with the transfer matrix $H(\omega) = (-\omega^2[M] + i\omega[C] + [K])^{-1}$, Eq. (1) yields the amplitude vector of the displacement response

$$\{X(\omega)\} = H(\omega)\{F(\omega)\} \quad (4)$$

Consider the substructure-superstructure system as being forced by wind excitation, which is idealized as a Gaussian zero-mean stationary process defined by the power spectral density function (PSD) of the force $S_{FF}(\omega)$. The PSD matrix of the displacement response is

$$S_{XX}(\omega) = H^*(\omega) S_{FF}(\omega) H(\omega) \quad (5)$$

where * is the complex conjugate transpose.

The RMS of the displacement response of each node can be evaluated through the numerical integration of the auto-spectral density function. The RMS of the displacement response is

$$\sigma_X = \sqrt{\int_{-\infty}^{\infty} S_{XX}(\omega) d\omega} \quad (6)$$

The amplitude vector of the acceleration response is

$$\{\ddot{X}(\omega)\} = -\omega^2 \{X(\omega)\} \quad (7)$$

Thus, the PSD matrix of the acceleration response can be obtained using Eq. (8).

$$S_{\ddot{X}\ddot{X}}(\omega) = \omega^4 S_{XX}(\omega) \quad (8)$$

The RMS of the acceleration response is

$$\sigma_{\ddot{X}} = \sqrt{\int_{-\infty}^{\infty} S_{\ddot{X}\ddot{X}}(\omega) d\omega} \quad (9)$$

2.2 Impedance function of a pile group

The impedance function of a pile group, in any vibration mode, can be calculated using the impedance function of a single pile in conjunction with dynamic interaction factors.

Typically, the impedance function of the single pile is expressed in the following simple form

$$K_{\alpha}^{[1]} = k_{\alpha}^{[1]} + i\omega c_{\alpha}^{[1]} \quad (10)$$

where $k_{\alpha}^{[1]}$ and $c_{\alpha}^{[1]}$ are the frequency-dependent stiffness and damping coefficient, respectively, and the index α denotes the direction, including horizontal, vertical, rocking and torsional directions. These stiffness and damping can be obtained from published solutions in the form of formulae and charts using Novak's plane-strain formulation (Novak 1974a, Novak and Howell 1977). At frequencies lower than the first natural frequency of the soil layer, only material damping remains because no progressive wave occurs to generate geometric damping (Novak and Sharnouby 1983).

Next, the dynamic interaction factors derived from a beam on a Winkler foundation model in conjunction with simplified wave propagation theory (Dobry and Gazetas 1988, Gazetas *et al.* 1991) are calculated as follows. The horizontal interaction factor for two floating piles in a homogeneous half-space is

$$\alpha_h(S, \theta) = \alpha_h(S, 0) \cos^2 \theta + \alpha_h\left(S, \frac{\pi}{2}\right) \sin^2 \theta \quad (11)$$

where $\alpha_h(S, 0) = (S/r_0)^{-1/2} \exp(-\beta\omega S/V_{La}) \exp(-i\omega S/V_{La})$ and $\alpha_h(S, \pi/2) = (S/r_0)^{-1/2} \exp(-\beta\omega S/V_s) \exp(-i\omega S/V_s)$; S is the distance between the axes of two piles; θ is the angle between the direction of loading and the line connecting the axes of the two piles; V_s is shear wave velocity and V_{La} is Lysmer's analog wave velocity, $V_{La} = 3.4V_s/[\pi(1-\nu)]$.

For vertical and rocking modes, pile motion is along the axial direction, and the interaction factors for two floating piles in a homogeneous half-space is

$$\alpha_v(S) = \left(\frac{S}{r_0}\right)^{-1/2} \exp(-\beta\omega S/V_s) \exp(-i\omega S/V_s) \quad (12)$$

Finally, the impedance function of a pile group is calculated by the method of superposition (El Naggar and Novak 1994, Makris *et al.* 1996). The horizontal impedance function of a pile group consisting of N piles is simply

$$K_x^{[G]} = K_x^{[1]} \sum_{i=1}^N \sum_{j=1}^N \varepsilon_{X(i,j)} \quad (13)$$

where $\varepsilon_X(i, j)$ is the inverse of the matrix $\alpha_h(i, j)$ obtained from Eq. (11).

The vertical impedance function of the group is also given by the equivalent expression

$$K_v^{[G]} = K_v^{[1]} \sum_{i=1}^N \sum_{j=1}^N \varepsilon_{Z(i,j)} \quad (14)$$

where $\varepsilon_Z(i, j)$ is the inverse of the matrix $\alpha_v(i, j)$ obtained from Eq. (12).

The rocking impedance function of the group can be derived using a similar analysis as follows

$$K_{\psi}^{[G]} = \sum_{i=1}^N K_{\psi}^{[1]} + K_v^{[1]} \sum_{i=1}^N x_i \sum_{j=1}^N x_j \varepsilon_{Z(i,j)} \quad (15)$$

where x_i is the distance of pile i from the axis about which rotation occurs. The rocking impedance function is derived from two components: the moments arising from unit rotations at the pile heads and the moments resulting from the vertical pile forces.

The torsional impedance function of the group can be derived as

$$K_t^{[G]} = \sum_{i=1}^N K_t^{[1]} + K_x^{[1]} \left(\sum_{i=1}^N x_i \sum_{j=1}^N x_j + \sum_{i=1}^N y_i \sum_{j=1}^N y_j \right) \varepsilon_{X(i,j)} \quad (16)$$

where x_i and y_i are the distances of pile i from the axis about which torsion occurs along the x-axis and y-axis, respectively, as depicted in Fig. 2. The torsional impedance function is derived from two components: the torque arising from unit torsions at the pile heads and the torque resulting from the horizontal pile forces. Similarly, the impedance function of pile group can be expressed in the form

$$K_{\alpha}^{[G]} = k_{\alpha}^{[G]} + i\omega c_{\alpha}^{[G]} \quad (17)$$

where $k_{\alpha}^{[G]}$ and $c_{\alpha}^{[G]}$ are the frequency-dependent stiffness and damping coefficients of the pile group, respectively.

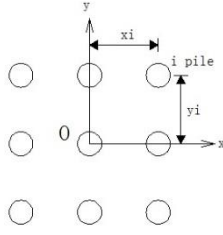


Fig. 2 Arrangement of the piles

2.3 Wind load

A 300-m building with cross-section dimensions of 50 m × 50 m is chosen as an example and the building is divided into 10 identical parts along the height. Wind loads on such building were obtained from synchronous pressure measurements conducted in the TJ-2 boundary-layer wind tunnel at Tongji University. The rigid 1:500 scale model of the building used in the tests was instrumented with a total of 200 pressure taps distributed on 10 levels along the height and 50 taps over each wall surface of the model. The sampling frequency adopted was 312.5 Hz, and a total 6000 data points were recorded during the time duration of approximately 19.2 s. The wind direction was defined as the direction from which the wind blows, measured clockwise from one main axis of the model. Due to the symmetry of the square cross section of the model, wind tunnel tests were conducted for 4 wind directions at 15-degree intervals (0°, 15°, 30°, and 45°). Multiple tests were conducted with wind speed profiles and turbulence intensities corresponding to the open and urban terrain conditions specified in the Load Code for the Design of Building Structures (GB 50009-2012 2012), as terrain B and terrain D, respectively. Adopting the exponential approximation, the exponents of the mean wind profiles were evaluated as $\alpha=0.16$ and $\alpha=0.30$ for open and urban terrain conditions, respectively. The turbulence intensities at the top of the target building model corresponding to a prototype height of 300 m were 5.8% and 8.6% for open and urban terrain conditions, respectively. The mean wind speeds at the top of the model were 10.49 and 9.60 m/s for open and urban terrain conditions, respectively. For the prototype building, a 10-min average reference wind speed at 10 meters above the ground in open terrain $V_r=29.7$ m/s was arbitrarily adopted. According to the exponential law adopted in the Load Code for the Design of Building Structures (GB 50009-2012 2012), this wind speed corresponds to a mean wind speed at the top $V_p=51.18$ and 46.45 m/s in open and urban terrain conditions, respectively.

According to the similitude criterion on the reduced frequency and pressure, the realistic pressure time histories at the prototype scale can be obtained from the measurements on the small-scale model as follows

$$\frac{n_m D_m}{V_m} = \frac{n_p D_p}{V_p} \Rightarrow \Delta t_p = \frac{1}{n_p} = \frac{D_p V_m}{D_m V_p n_m} \quad (18)$$

where n is the frequency of the forcing function, V is the mean wind speed, D is the side length of the building cross-

section and Δt is the time interval. The subscript m refers to the model, and the subscript p refers to the prototype.

$$\begin{aligned} \frac{F_p}{F_m} &= \frac{0.5\rho V_p^2 h_p D_p}{0.5\rho V_m^2 h_m D_m} = \left(\frac{V_p}{V_m}\right)^2 \left(\frac{1}{C_1}\right)^2 \\ \Rightarrow F_p &= \left(\frac{V_p}{V_m}\right)^2 \left(\frac{1}{C_1}\right)^2 F_m \end{aligned} \quad (19)$$

where F is the pressure, ρ is the air density, h is the height of each level and C_1 is the length scale. According to Eq. (18), the time intervals Δt between two subsequent measurement time stations of the pressure coefficients are 0.328 s and 0.331 s for open and urban terrain conditions, respectively.

The translational forces and torque at each part are determined by integrating wind pressure within the tributary area. Fig. 3 shows the power spectral densities (PSDs) of the time histories of along-wind and across-wind forces and torsional moments of the 2nd-9th part for the open terrain, 0° wind direction condition. For the across-wind force, the highest spectral values are located at approximately 0.1013 Hz and correspond to vortex shedding. For the torsional moments, the peaks due to vortex shedding are also at approximately 0.1013 Hz.

3. Verification of the proposed calculation models

Different from the traditional fixed base model for wind-induced responses analysis, the proposed calculation model has a single-node soil-foundation element (linear elastic) at the base of supertall building to consider SSI. To validate the single-node soil-foundation element, comparison was carried out between the proposed calculation models and analogue finite element models using the software package ABAQUS. The finite element

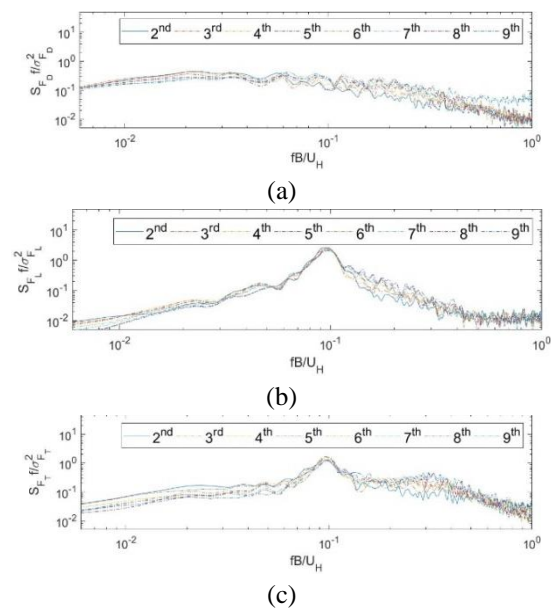


Fig. 3 Power spectral densities of (a) along-wind forces, (b) across-wind forces and (c) torsional moments on each part

model used continuum elements to model the soil-foundation system, which is more complicated than the single-node soil-foundation element in the proposed calculation model. The finite element model adopted lumped-mass model for the superstructure as the proposed calculation model does. The finite element model has more than 2.4×10^4 elements and very closely-spaced modes of vibration. Thus, instead of frequency-domain analysis, time-domain analysis is adopted in the finite element model. Time history of wind-induced responses was firstly calculated in finite element models and then transferred to power spectra to compare with results in proposed calculation models.

3.1 Finite element models

The ABAQUS version 6.14 environment was used to enable 3D analyses of the soil-pile group-superstructure system (Sinha and Hanna 2017). The model of this integrated system was elastic. The superstructure was modeled using Timoshenko beam elements and lumped masses. The soil zone consisted of classical elements (the finite part) surrounded by infinite elements (the infinite part) to account for the unbounded nature of the ground (Javan *et al.* 2014). The piles, the raft and the finite section of soil were modeled by C3D20R (continuous, twenty nodes with reduced integration) elements, and the infinite section of soil was modeled by CIN3D8 (continuous with eight nodes) infinite elements, which can eliminate reflection on the boundary. Pairs of surfaces of soil and piles, and surfaces of piles and the raft were perfectly tied. The node at the base of the superstructure and the reference node tied with the top surface of the raft were completely coupled. Boundary effects were further avoided by setting the horizontal length of the finite soil zone as 50 times the pile diameter and the vertical depth as 3 times the pile length. Moreover, the dimensions of the infinite soil zone were the same as those of the finite soil zone. No translation was allowed in the bottom nodes of the finite soil zone. Fig. 4 presents the meshed soil-foundation-superstructure system and the pile group foundation.

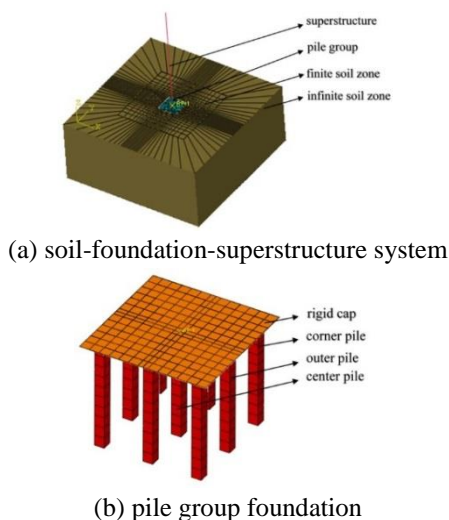


Fig. 4 Finite element model

Table 1 Static top displacement

	Proposed calculation model (SSI)	Finite element model (SSI)
Along-wind (m)	0.2092	0.2076
Across-wind (m)	0.005062	0.005012

3.2 Comparison between the proposed calculation models and the finite element models

As mentioned in Section 2.3, a 300-m supertall building with cross-section dimensions of $50 \text{ m} \times 50 \text{ m}$ is chosen as an example. Assuming the building is 75 stories with story height of 4 m and the mass of $1.3 \times 10^3 \text{ kg/m}^2$ uniformly distributed over each floor surface. The building is divided into 10 identical parts and modeled as a lumped-mass system with each node mass of $2.4375 \times 10^7 \text{ kg}$. Due to the symmetric behavior along the horizontal x- and y-directions, the flexural moments of inertia of each node along the x- and y-directions are both $5.0781 \times 10^9 \text{ kg}\cdot\text{m}^2$. The torsional moments of inertia of each node is $1.0156 \times 10^{10} \text{ kg}\cdot\text{m}^2$. Ten identical Timoshenko beam elements, with 6 DOFs per node, are used to provide the stiffness of the building. The first natural frequencies in the x- and y-directions are both 0.1727 Hz, which satisfies the empirical formula for the natural frequencies of tall buildings suggested in the Load Code for the Design of Building Structures (GB 50009-2012 2012). The Rayleigh model is adopted to describe the structural damping properties of the equivalent beams, assuming a damping ratio of 3% of the critical damping.

Considering SSI, a 3×3 pile group is used in this numerical example. The piles have a diameter of $d_p=3.85 \text{ m}$, length of $l_p=57.75 \text{ m}$, and separation of $s=19.25 \text{ m}$ and are connected by a 0.1 m thick, rigid, massless cap with width of $B_f=50.05 \text{ m}$. The mechanical properties of the piles are Young's modulus $E_p=441,000 \text{ MPa}$, Poisson's ratio $\nu_p=0.25$, unit mass $\rho_p=2500 \text{ kg/m}^3$ and damping $\xi_p=0$. This pile group stands in a $H=173.25 \text{ m}$ thick soil layer with Young's modulus $E_s=441 \text{ MPa}$, Poisson's ratio $\nu_s=0.40$, unit mass $\rho_s=1750 \text{ kg/m}^3$ and material hysteric damping $\xi_s=0.05$.

To validate the stiffness of single-node soil-foundation element, static top displacement calculated from these two models are compared. The mean wind load in the along-wind, across-wind and torsional directions for the 0° wind direction and open terrain condition acquired from the wind tunnel tests (as mentioned in Section 2.3) are applied as static wind loads in the 10 nodes of superstructure as point loads. The static top displacements of the soil-pile group-superstructure system of the proposed calculation model and the finite element model are compared in Table 1. The results of the two models are consistent.

To validate the damping of single-node soil-foundation element, dynamic wind-induced responses calculated from these two models are also compared. The wind loads in the along-wind, across-wind and torsional directions applied in the soil-pile group-superstructure system of the infinite element model for the time-domain analysis; the PSDs of the wind loads are obtained from the time histories of the

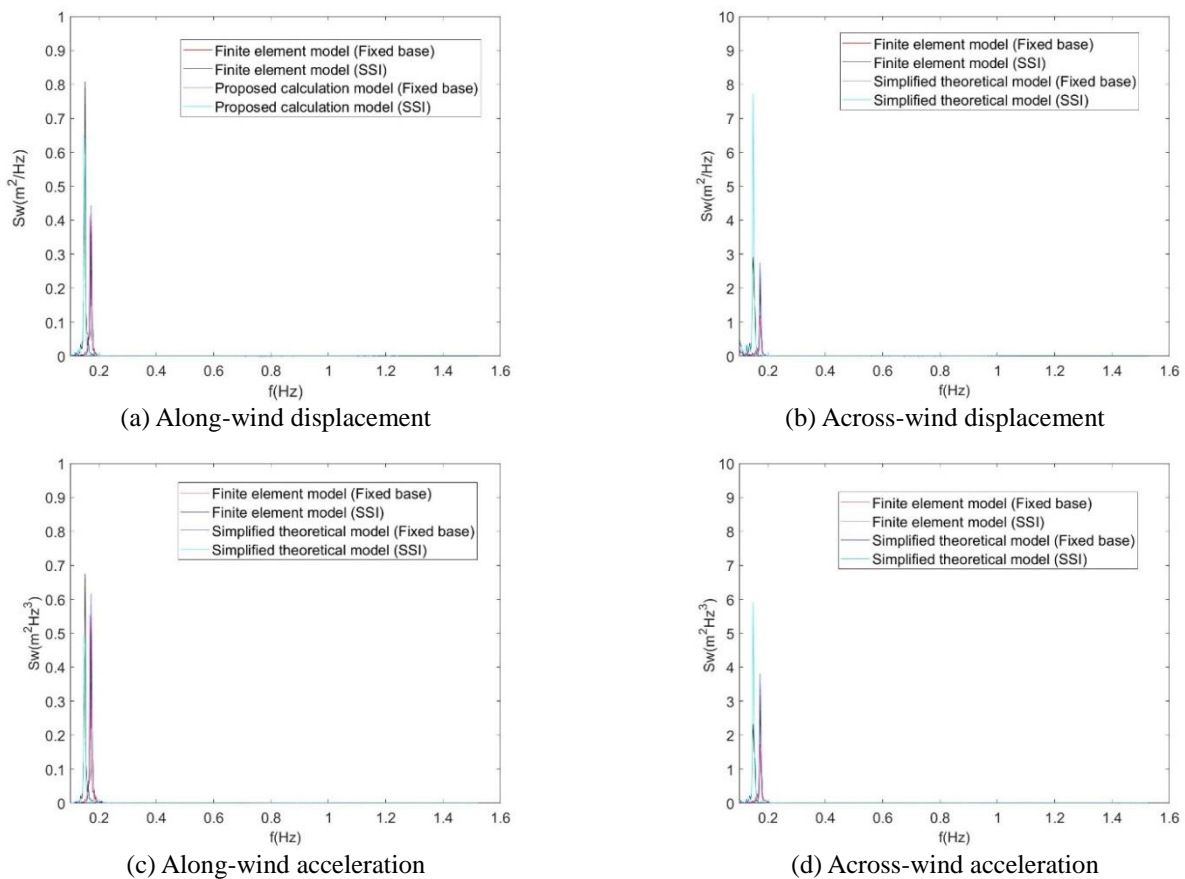


Fig. 5 PSDs of the wind-induced responses on top of the supertall building

wind loads using the frequency Fourier transform, and frequency domain analyses are then conducted for the same coupled system in the proposed calculation model. However, except for different modeling approaches for soil-foundation, dynamic analysis methods are also different in these two models, which are the Newmark integration method for time-domain analysis and the transfer function method for frequency-domain analysis. On the other hand, fixed-base building in these two models are the same, thus wind-induced responses from time-domain analysis in the finite element model and frequency-domain analysis in the proposed calculation model are also compared to understand the different results caused by the different dynamic analysis method.

The PSD values of the displacements and accelerations on top of the supertall building with the fixed base and with the flexible base computed using the finite element method and using the proposed calculation method are given in Fig. 5. The agreement in the first peak response between the two approaches is found to be very good. The RMS of the top displacements and accelerations obtained from the finite element model and the proposed calculation model are compared in Table 2. For the superstructure with the fixed base, the percentage differences of the RMS of the along-wind top displacement, along-wind top acceleration, across-wind top displacement and across-wind top acceleration between the finite element model and the proposed

calculation model are 2.7%, 5.2%, 13.6% and 17.7%, respectively. For the superstructure with the fixed base, difference in responses between these two models result from the different dynamic analysis methods. For the soil-pile group-superstructure system, the percentage differences of the responses between the finite element model and the responses between the finite element model and the proposed calculation model are similar as those of the superstructure with fixed base. Thus, the difference also results from the different analytical methods adopted in the time domain and frequency domain, and the proposed calculation model is in good agreement with the finite element model. Moreover, the percentage differences in the RMS of the along-wind and across-wind responses between the frequency-domain analysis and the time-domain analysis are less than 10% and 20%, respectively, which are acceptable. Therefore, the proposed calculation model for the frequency-domain analysis can accurately compute the wind-induced responses of supertall buildings with consideration of SSI.

4. Parametric analysis

Considering four wind load directions (0° , 15° , 30° and 45°) and two terrain conditions (open terrain and urban terrain), wind loads were applied to a 300-m supertall

Table 2 RMS values of the top responses

	Proposed calculation model (Fixed base)	Finite element model (Fixed base)	Percentage difference (Fixed base)	Proposed calculation model (SSI)	Finite element model (SSI)	Percentage difference (SSI)
RMS along-wind displacement (m)	0.0579	0.0563	2.6%	0.0750	0.0797	6.3%
RMS across-wind displacement (m)	0.1482	0.1281	13.6%	0.2434	0.2064	15.2%
RMS along-wind acceleration (m/s^2)	0.0650	0.0617	5.2%	0.0629	0.0691	9.8%
RMS across-wind acceleration (m/s^2)	0.1598	0.1315	17.7%	0.1979	0.1682	15.0%

building. Proposed calculation models were constructed to analyse the wind-induced responses of this building considering SSI in the frequency domain. The soil, pile group and supertall building parameters were given in section 3.2 and the wind load data were given in section 2.3 in detail. The first natural frequency and the responses of the supertall building, such as the static displacement, RMS of displacement and acceleration on the top of the building, were analysed. The variations of the dynamic property and the response of the supertall building with the flexible base from those of the supertall building with the fixed base were computed. The effect of soil shear wave velocity (from 200 m/s to 600 m/s) and soil material damping (from 1% to 5%) on the above variations was studied.

4.1 Variation of the natural frequency of the supertall building

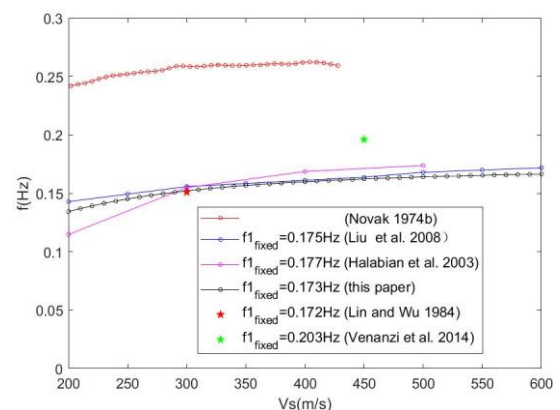
The variation of the first natural frequency of the supertall building with the soil shear wave velocity is shown in Fig. 6(a). As the shear wave velocity decreases from 600 m/s to 200 m/s, the first natural frequency decreases from 0.1664 Hz to 0.1343 Hz. The first natural frequency of the supertall building with the fixed base is 0.1726 Hz. Moreover, the results from other researchers, which are also given in Fig. 6(a), are consistent with the results obtained in this research. The SSI decreases the first natural frequency, and the effect of SSI becomes more pronounced as the soil shear wave velocity decreases. Due to the flexibility of the soil-foundation, the stiffness of the superstructure with the flexible base is less than that of the superstructure with the fixed base; thus, the first natural frequency of the superstructure with the flexible base is less than that with the fixed base. Moreover, with the decrease of the soil shear wave velocity (representing a softer soil), the stiffness of the coupled system decreases, leading to the decrease of the first natural frequency.

The first natural frequency of the supertall building with the flexible base is normalized to that of the supertall building with the fixed base. The variation of the normalized first natural frequency of the supertall building with the soil shear wave velocity is shown in Fig. 6(b). Despite the foundation type and the height of supertall building in this research being different from those in other research studies, the decreasing ratio of the first natural frequency with the decrease of the soil shear wave velocity in this research is found to be consistent with that in the

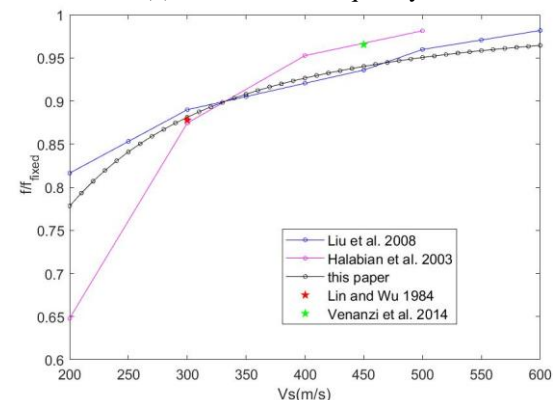
other research studies. When the soil shear wave velocity is 600 m/s, the first natural frequency of the supertall building with the flexible base is 96.4% of that with the fixed base; when the soil shear wave velocity is 200 m/s, the first natural frequency of the supertall building with the flexible base is 77.8% of that with the fixed base.

4.2 Variation of the static displacement at the top of the supertall building

Under different wind directions and different terrain conditions, the variation of the static top displacement with the soil shear wave velocity is shown in Fig. 7.



(a) First natural frequency



(b) Normalized first natural frequency

Fig. 6 Variation of the first natural frequency with the soil shear wave velocity

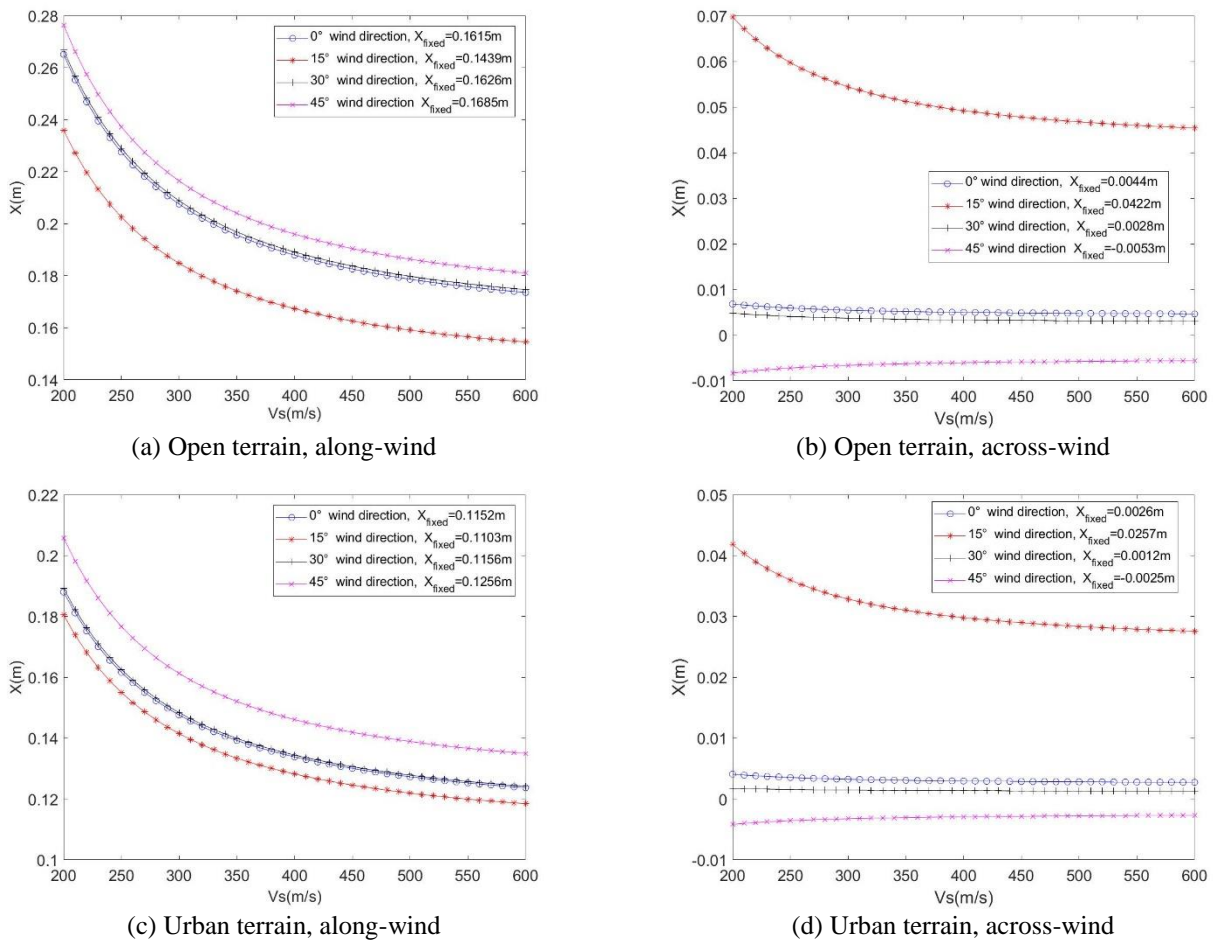


Fig. 7 Variation of the static displacement with the soil shear wave velocity

The static top displacements in open terrain are observed to be larger than the displacements in urban terrain, and the along-wind static top displacements are larger than the across-wind displacements. The difference of the along-wind static top displacements in the different wind direction is small. However, the across-wind static top displacements under 15° wind direction is much higher than that under other wind directions because under this wind direction, the asymmetry of the flow field leads to vortex shedding, and the lift force increases. For all analysis cases under different terrain and wind directions, the effect of SSI is to increase the static top displacement, and with the decrease of soil shear wave velocity, the effect of SSI is more significant. Due to the soil flexibility, the stiffness of the soil-pile group-superstructure system decreases and the response increases; if the soil is softer, the stiffness of the coupled system is reduced, and the response is more prominent.

Similarly, the static top displacement of the supertall building with the flexible base is normalized to that with the fixed base. The variation of the normalized along-wind static top displacement with soil shear wave velocity is shown in Fig. 8(a) and is compared with the results from Novak (1974b). For all analysis cases under different terrains and wind directions, the general trends for the variation of the along-wind static top displacement with soil

shear wave velocity are found to be the same. As the soil shear wave velocity decreases from 600 m/s to 200 m/s, the percentage variation of the along-wind static top displacement of the supertall building with the flexible base from that with the fixed base increases from 7.4% to 63.9%. The result is higher than that reported by Novak since the heights of the supertall buildings in Novak's work are only 40 m and 80 m, i.e., much shorter than that in this research. Fig. 8(b) shows that as the soil shear wave velocity decreases from 600 m/s to 200 m/s, the percentage variation of the across-wind static top displacement of the supertall building with the flexible base from that with the fixed base increases from 6.9%-8.3% to 56.2%-63.9%.

4.3 Variation of the RMS displacement at the top of the supertall building

In different wind directions and terrain conditions, the effects of SSI on the RMS top displacement are similar. The RMS top displacement of the supertall building with the flexible base is normalized to that with the fixed base. In the 0° wind direction and open terrain condition, the variation of the normalized RMS top displacement with the soil shear wave velocity and soil material damping are shown in Figs. 9 and 10, respectively. Fig. 9 shows that due to the soil-

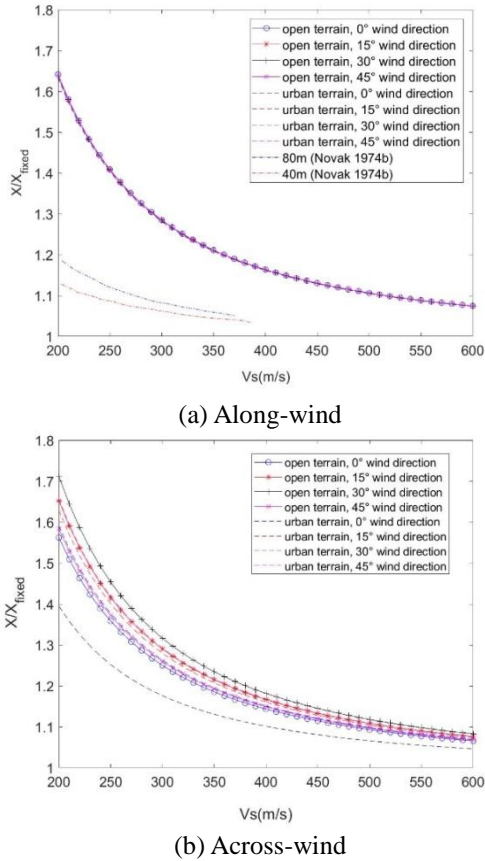


Fig. 8 Variation of the normalized static displacement with the soil shear wave velocity

foundation flexibility, the RMS top displacement of the supertall building with the flexible base is larger than that with the fixed base. In addition, as the soil shear wave velocity decreases, the percentage increase of the RMS increases. The reason is that when the soil shear wave velocity is small, the stiffness and radiation damping of the soil are small, resulting in small stiffness and damping of the whole soil-pile group-superstructure system. Therefore, the dynamic responses on the top of the supertall building are large. As the soil shear wave velocity decreases from 600 m/s to 200 m/s, the percentage variations of the along-wind and across-wind RMS top displacements of the supertall building with the flexible base relative to those with the fixed base increase from 12%-15.1% to 106.6%-192.9% and from 9.3%-11.6% to 211.2%-331.8%, respectively. For very dense soil or soft rock ($366 \text{ m/s} \leq V_s < 600 \text{ m/s}$) (ASCE/SEI Standard 7-10 2010), the percentage variations are small (RMS top displacement in the along-wind and across-wind directions, increase around 22.4% and 22.7%, respectively), but for stiff soil ($200 \text{ m/s} \leq V_s < 366 \text{ m/s}$), the percentage variations observed are high. When the soil is really weak ($V_s = 200 \text{ m/s}$), the percentage increase is up to 139.9% and 257.6% in along-wind and across-wind directions.

When the soil shear wave velocity is 300 m/s, the percentage increases of the along-wind and across-wind RMS top displacements are 35.5%-54.6% and 71.5%-94.5%, respectively. Lin and Wu (1984) also found that the

along-wind RMS top displacement of a 160-m supertall building with a flexible base is 20.5%-29.2% larger than that with a fixed base when the soil shear wave velocity is 300 m/s, in agreement with the result in this research. When the soil shear wave velocity is 450 m/s, the percentage increases of the along-wind and across-wind RMS top displacements are 20.5%-29.2% and 24.9%-31.1%, respectively. Venanzi *et al.* (2014) found that the across-wind RMS top displacements of a 180-m supertall building with a flexible base in open and urban terrain conditions are 38% and 43% larger than those with a fixed base when the soil shear wave velocity is 450 m/s, in agreement with the result in this research.

Fig. 10 shows that with the decrease of the soil material damping, the percentage increase of the RMS increases. The reason is that when the soil material damping is small, the damping of a single pile (especially under low frequency vibration) and the interaction factors of the pile group are small, leading to small stiffness and damping of the soil-foundation system and large dynamic responses on the top of supertall building. In addition, when the soil shear wave velocity is large, the variation of the RMS top displacement with the soil material damping is not prominent. However, when the soil wave velocity is small (e.g., 200 m/s), the variation is significant since when the soil becomes soft, the soil radiation damping becomes small, and the soil material damping becomes the main source of soil damping. When the soil shear wave velocity is 200 m/s, with the decrease of the soil material damping ratio from 5% to 1%, the percentage increase of the along-wind and across-wind RMS top displacement increases from 106.7% to 192.9% and from 210.2% to 337.4%, respectively; when the soil shear wave velocity is in the range of 300 m/s to 600 m/s, the variation of the RMS displacement with the soil material damping is not prominent. Especially, when the soil shear wave velocity is 600 m/s, with the decrease of the soil material damping ratio from 5% to 1%, the percentage increase of the along-wind and across-wind RMS top displacement only increases from 12.0% to 16.2% and from 9.3% to 11.6%, respectively.

4.4 Variation of the RMS acceleration at the top of the supertall building

The variation of the RMS top acceleration in the 0° wind direction and open terrain condition with soil shear wave velocity is shown in Fig. 11. Fig. 11 reveals that the effect of SSI is to increase RMS top acceleration, and the effect of SSI is more pronounced as the soil shear wave velocity decreases. From Fig. 11, we can see when the soil shear wave velocity decreases from 600 m/s to 200 m/s, the percentage variation of the along-wind and across-wind RMS top acceleration of the supertall building with the flexible base from that with the fixed base increases from 4%-8.9% to 25.2%-87% and from -2.4%-0.7% to 102.4%-191.4%, respectively. For very dense soil or soft rock, the percentage increase in along-wind and across-wind directions is 10.7% and 7.7%, respectively; for stiff soil, the percentage increase is 15.7% and 59.2%.

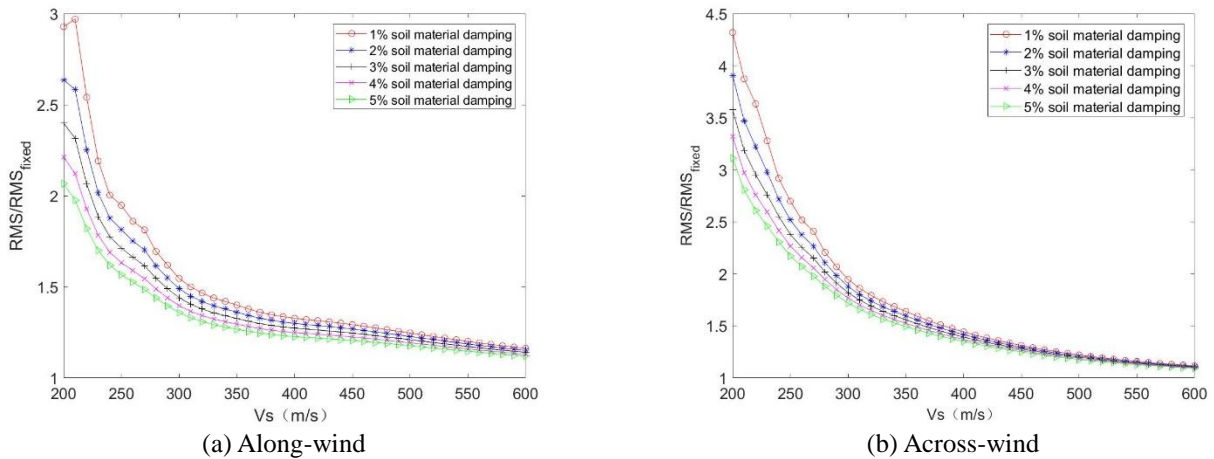


Fig. 9 Variation of the normalized RMS top displacement with the soil shear wave velocity

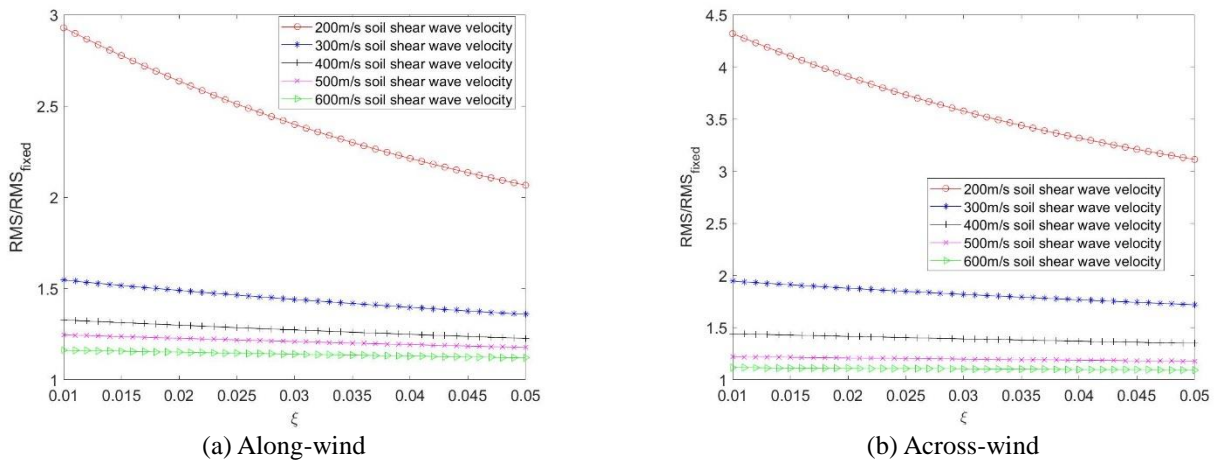


Fig. 10 Variation of the normalized RMS top displacement with the soil material damping

The variation of the normalized RMS top acceleration with the soil material damping is shown in Fig. 12. According to Fig. 12, as soil material damping decreases, the RMS top acceleration increases. When the soil shear wave velocity is 200 m/s, with the decrease of the soil material damping ratio from 5% to 1%, the percentage increase of the along-wind and across-wind RMS top accelerations increase from 25.2% to 87% and from 102.4% to 194.1%, respectively; when the soil shear wave velocity is in the range of 300 m/s to 600 m/s, the variation of RMS acceleration with soil material damping is not prominent. Especially, when the soil shear wave velocity is 600 m/s, with the decrease of the soil material damping ratio from 5% to 1%, the percentage increase of the along-wind RMS top acceleration only increases from 4.0% to 8.9% and the percentage increase of the across-wind RMS top acceleration nearly stays at zero.

5. Conclusions

In this paper, a calculation model for frequency-domain analysis was adopted, soil-pile group-supertall building interaction models were built, and the effect of SSI on the first natural frequency, static displacement, RMS of displacement and acceleration on top of a supertall building in different terrain, wind direction, soil shear wave velocity and soil material damping conditions were studied. The conclusions drawn from this study are summarized as follows:

- Due to the flexibility of the soil-foundation, the stiffness of a superstructure with a flexible base was found to be less than that of a superstructure with a fixed base. Moreover, the first natural frequency decreased with decreasing soil shear wave velocity. When the shear wave velocity decreased from 600 m/s to 200 m/s, the first natural frequency of the supertall building with the flexible base decreased from 0.1664 Hz to 0.1343 Hz, compared with the first natural frequency 0.1726 Hz of the supertall building with the fixed base.

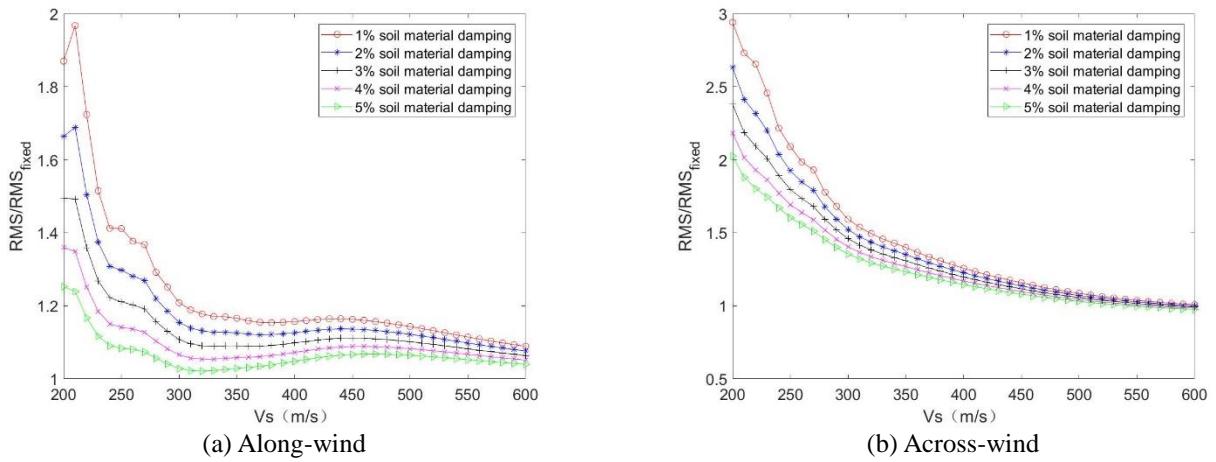


Fig. 11 Variation of the normalized RMS top acceleration with the soil shear wave velocity

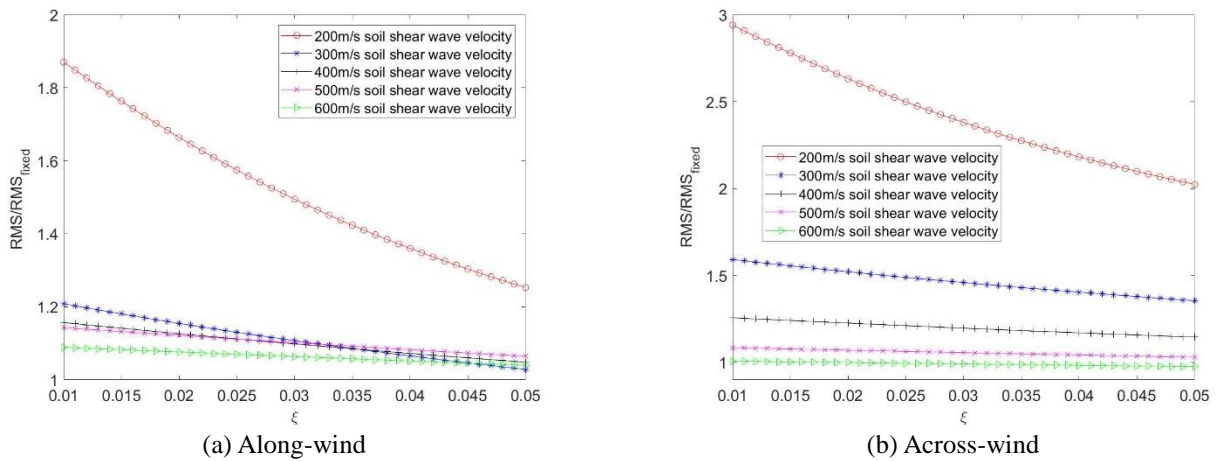


Fig. 12 Variation of the normalized RMS top acceleration with the soil material damping

- In different wind directions and terrain conditions, the effect of SSI on static displacement was found to be similar. It increased the static top displacement, and became more significant as soil shear wave velocity decreased. As the soil shear wave velocity decreased from 600 m/s to 200 m/s, the percentage variations of the along-wind and the across-wind static top displacements of the supertall building with the flexible base compared with those of the supertall building with the fixed base increased from 7.4% to 63.9% and from 7.6% to 60.1%, respectively.

- The effect of SSI that increases the RMS of the top displacement was also similar in different wind directions and terrains. And soil shear wave velocity affected SSI effect greatly. For very dense soil or soft rock, the percentage variations were small (RMS top displacement in the along-wind and across-wind directions, increased around 22.4% and 22.7%, respectively), but for stiff soil, the percentage variations observed were high. When the soil was really weak, the percentage increase was up to 139.9% and 257.6% in along-wind and across-wind directions. The high percentage variation observed in the

case of stiff soil proves that SSI effect may dramatically increase wind-induced responses of super-tall building with pile group foundation, when soil is weak. Moreover, when the soil shear wave velocity was small, the variation of the RMS top displacement with soil material damping was prominent. Thus, when calculating wind-induced responses of supertall buildings considering SSI for soft soil, the value of soil material damping should be given very carefully.

- The effect of SSI on the RMS of the top acceleration was similar to that on the RMS of the top displacement. For very dense soil or soft rock, the percentage increase in along-wind and across-wind directions is 10.7% and 7.7%, respectively; for stiff soil, the percentage increases is 15.7% and 59.2%.

SSI effect can increase wind-induced displacement and acceleration responses on the top of supertall building founded on pile group, and when soil is weak, the increase percentage is high. Thus, SSI should be considered when designing wind-resistant supertall buildings and the value of soil shear wave velocity and soil material damping should be given carefully.

Acknowledgments

The authors gratefully acknowledge support from the National Natural Science Foundation of China (91215302, 90715040) and the Key Project of State Key Laboratory of Disaster Reduction in Civil Engineering (SLDRCE15-A-04).

References

- Adhikari, S. and Bhattacharya, S. (2011), "Vibration of wind-turbines considering soil-structure interaction", *Wind Struct.*, **14**(2), 85-112.
- ASCE/SEI Standard 7-10 (2010), Minimum Design Loads for Buildings and Other Structures, American Society of Civil Engineers; Reston, VA, USA.
- Dobry, R. and Gazetas, G. (1988), "Simple method for dynamic stiffness and damping of floating pile groups", *Geotechnique*, **38**(4), 557-574.
- Galsworthy, J.K. and El Naggar, M.H. (2000), "Effect of foundation flexibility on the cross-wind response of R/C chimneys with free standing liners", *Can. Geotech. J.*, **37**(3), 676-688.
- Gazetas, G., Fan, K., Kaynia, A. and Kausel, E. (1991), "Dynamic interaction factors for floating pile groups", *J. Geotech. Eng.*, **117**(10), 1531-1548.
- GB 50009-2012 (2012), Load Code for the Design of Building Structures, China Architecture and Building Press; Beijing, China (in Chinese).
- Gorski, P. and Chmielewski, T. (2008), "A comparative study of along and cross-wind responses of a tall chimney with and without flexibility of soil", *Wind & Structures An International Journal*, **11**(2), 121-135.
- Halabian, A.M., El Naggar, M.H. and Vickery, B.J. (2003), "Reliability analysis of wind response of flexibly supported tall structures", *Struct. Des. Tall Spec.*, **12**(1), 1-20.
- Howell J.F. (1978), "Soil-structure interaction under wind loading", Ph.D. Dissertation, Western University of Ontario, London.
- Irwin, P.A. (2009), "Wind engineering challenges of the new generation of super-tall buildings", *J. Wind Eng. Ind. Aerod.*, **97**(7), 328-334.
- Javan, M.H., Haghshenas, S.S., Javan, M.H. and Jalilvand, P. (2014), "Investigation of the effect of mass super structure in reaction single micropile under dynamic loading", *Geotech. Special Publication*, **240**(2014), 425-432.
- Jayalekshmi, B.R., Jisha, S.V. and Shivashankar R. (2015), "Wind load analysis of tall chimneys with piled raft foundation considering the flexibility of soil", *Int. J. Adv. Struct. Eng.*, **7**(2), 95-115.
- Jisha, S.V., Jayalekshmi, B.R. and Shivashankar, R. (2013), "Evaluation of the effect of soil-structure interaction on the raft of tall reinforced concrete chimneys under across wind load", *Proceedings of the 8th Asia-Pacific Conference on Wind Engineering*, Chennai, India, December.
- Liu, M.Y., Chiang, W.L., Hwang, J.H. and Chu, C.R. (2008), "Wind-induced vibration of high-rise building with tuned mass damper including soil-structure interaction", *J. Wind Eng. Ind. Aerod.*, **96**(6-7), 1092-1102.
- Lin, Y.K. and Wu, W.F. (1984), "Along-wind motion of building on compliant soil", *J. Eng. Mech.*, **110**(1), 1-19.
- Makris, M., Gazetas, G. and Delis, E. (1996), "Dynamic soil-pile foundation-structure interaction: records and predictions", *Geotechnique*, **46**(1), 33-50.
- El Naggar, M.H. and Novak, M. (1994), "Nonlinear lateral interaction in pile dynamics", *J. Geotech. Eng.*, **14**(4), 678-696.
- Novak, M. (1974a), "Dynamic stiffness and damping of piles", *Can. Geotech. J.*, **11**(4), 574-598.
- Novak, M. (1974b), "Effect of soil on structural response to wind and earthquake", *Earthq. Eng. Struct. D.*, **3**(1), 79-96.
- Novak, M. and Howell, J.F. (1977), "Torsional vibrations of pile foundations", *J. Geotech. Eng. Div.*, **103**, 271-285.
- Novak, M. and Sharmouby, B.E. (1983), "Stiffness constants of single piles", *J. Geotech. Eng.*, **109**(7), 961-974.
- Novak, M. and Hifnawy, L.E. (1988), "Structural response to wind with soil-structure interaction", *J. Wind Eng. Ind. Aerod.*, **28**(1), 329-338.
- Rong, X.N., Xu, R.Q., Wang, H.Y. and Feng, S.Y. (2017), "Analytical solution for natural frequency of monopole supported wind turbine towers", *Wind Struct.*, **25**(5), 459-474.
- Shirzadeh, R., Devriendt, C., Bidakhvidi, M.A. and Guillaume, P. (2013), "Experimental and computational damping estimation of an offshore wind turbine on a monopile foundation", *J. Wind Eng. Ind. Aerod.*, **120**(120), 96-106.
- Sinha, A. and Hanna, A.M. (2017) "3D numerical model for piled raft foundation", *Int. J. Geomech.*, **17**(2), 04016055.
- Venanzi, I., Salciarini D. and Tamagnini C. (2014), "The effect of soil-foundation-structure interaction on the wind-induced response of tall buildings", *Eng. Struct.*, **79**(4), 117-130.
- Viladkar, M.N., Bhargava, P. and Godbole, P.N. (2006), "Static soil-structure interaction response of hyperbolic cooling towers to symmetrical wind loads", *Eng. Struct.*, **28**(9), 1236-1251.
- Wolf, J.P. (1985), *Dynamic Soil-structure Interaction*, Prentice-Hall, Inc., Englewood Cliffs, NJ, USA.
- Xu, Y. L. and Kwok, K.C.S. (1992), "Wind-induced response of soil-structure-damper systems", *J. Wind Eng. Ind. Aerod.*, **43**(1-3), 2057-2068.

CC